



# CHORUS

This is the accepted manuscript made available via CHORUS. The article has been published as:

## Nanodopant-Induced Band Modulation in $\text{AgPb}_{\{m\}}\text{SbTe}_{\{2+m\}}$ -Type Thermoelectrics

Yi Zhang, Xuezhi Ke, Changfeng Chen, Jihui Yang, and Paul R. C. Kent

Phys. Rev. Lett. **106**, 206601 — Published 20 May 2011

DOI: [10.1103/PhysRevLett.106.206601](https://doi.org/10.1103/PhysRevLett.106.206601)

# Nanodopant-Induced Band Modulation in $\text{AgPb}_m\text{SbTe}_{2+m}$ -Type Thermoelectrics

Yi Zhang,<sup>1</sup> Xuezhi Ke,<sup>2,1</sup> Changfeng Chen,<sup>1</sup> Jihui Yang,<sup>3</sup> and Paul R. C. Kent<sup>4</sup>

<sup>1</sup>*Department of Physics and HiPSEC, University of Nevada, Las Vegas, Nevada 89154, USA*

<sup>2</sup>*Department of Physics, East China Normal University, Shanghai 200062, China*

<sup>3</sup>*Electrochemical Energy Research Lab, GM R&D Center, Warren, Michigan 48090, USA*

<sup>4</sup>*Center for Nanophase Materials Sciences, Oak Ridge National Laboratory, Oak Ridge, Tennessee 37831, USA*

(Dated: April 20, 2011)

The structure-property relation is a key outstanding problem in the study of nanocomposite materials. Here we elucidate the fundamental physics of nanodopants in thermoelectric nanocomposites  $\text{XPb}_m\text{YTe}_{2+m}$  ( $X=\text{Ag,Na}$ ;  $Y=\text{Sb,Bi}$ ). First-principles calculations unveil a sizable band-gap widening driven by nanodopant-induced lattice strain and a band split-off mainly caused by the spin-orbit interaction in nanodopant. Boltzmann transport calculations on  $\text{PbTe}$  with modified band mimicking nanodopant-induced modulations show significant but competing effects on high-temperature electron transport behavior. These results offer insights for understanding experimental findings and optimizing thermoelectric properties of narrow band-gap semiconductor nanocomposites.

PACS numbers: 71.20.-b, 71.28.+d, 72.15.Jf

A hallmark of semiconductor physics is effective modulation of electronic structure and transport properties by doping [1]; however, the impact of nanoscale dopants remains largely unknown. Recent advances on doped lead chalcogenides show that superior thermoelectric (TE) figure of merit  $ZT = S^2\sigma T/(\kappa_e + \kappa_p)$  can be achieved when such nanodopants are introduced [2–10]. Here,  $S$ ,  $\sigma$ ,  $T$ ,  $\kappa_e$ , and  $\kappa_p$  are thermopower, electrical conductivity, absolute temperature, electron, and lattice thermal conductivity, respectively. These nanodopants reduce  $\kappa_p$  via enhanced phonon scattering [11], thus improving  $ZT$ ; their effect on thermopower has also been examined [2, 10, 12], but a full understanding is impeded by a lack of knowledge about the electronic structure of the nanocomposites. Previous calculations of  $\text{AgPb}_m\text{SbTe}_{2+m}$  (LAST) [13–16] are constrained to small supercell models and, consequently, are unable to assess the impact by the experimentally observed nanodopants. Most recent studies have identified the microstructure of  $\text{AgPb}_m\text{SbTe}_{2+m}$  [17, 18], making it possible to tackle the challenge of elucidating the impact of nanodopants on the electronic structure and TE properties.

In this Letter, we report first-principles calculations of the electronic structures of LAST-type nanocomposites  $\text{XPb}_m\text{YTe}_{2+m}$  ( $X=\text{Ag, Na}$ ;  $Y=\text{Sb, Bi}$ ). We also performed Boltzmann transport calculations on  $\text{PbTe}$  with band modifications to mimic the nanodopant-induced band modulations. For electronic-structure calculations, we employ a supercell containing 1000 atoms that can accommodate nanodopants of comparable size (2 to 3 nanometers) as observed in experiments [17]. Our results show that nanodopants induce strong modulations on the electronic structure of the host narrow-gap semiconductor  $\text{PbTe}$ , leading to a sizable widening of the band gap and a band splitting at the conduction band minimum (CBM). The increased band gap drives an enhancement of thermopower and power factor; however,

the band splitting reduces these quantities. The results explain the puzzling experimental findings [2, 10–12] of the limited influence of nanodopants on thermopower and power factor despite their large effects on thermal conductivity, and offer insights into the underlying physics in these narrow-gap semiconductor nanocomposites.

Our electronic structure calculations were performed using the generalized gradient approximation by Perdew and Wang [19] as implemented in the VASP package [20]. The projector augmented wave method [21] is used with a cutoff energy of 400 eV. Scalar relativistic effect and spin-orbit interaction (SOI) are included in band structure calculations. The structure of  $\text{AgSbTe}_2$  nanoprecipitates in the 1000-atom supercell (see Fig. 1) is obtained in the same way as previously reported [17]; the same approach is used to determine the structures of  $\text{AgPb}_m\text{BiTe}_{2+m}$  (LBST),  $\text{NaPb}_m\text{SbTe}_{2+m}$  (LANT), and  $\text{NaPb}_m\text{BiTe}_{2+m}$  (LBNT). All the structures are fully relaxed by non-SOI calculations as previously reported [17]. The WIEN2K [22] and BOLTZTRAP [23] package are used to evaluate the transport coefficients. The electrical conductivity tensor is defined as [23]  $\sigma_{\alpha\beta}(T, \mu) = \frac{1}{\Omega} \int \sigma_{\alpha\beta}(\epsilon) \left[ -\frac{\partial f_{\mu}(T, \epsilon)}{\partial \epsilon} \right] d\epsilon$ , where  $f$  and  $\mu$  are the Fermi function and chemical potential, respectively. The thermopower is given by  $S_{ij} = (\sigma^{-1})_{\alpha i} v_{\alpha j}$ , where  $v_{\alpha\beta}(T, \mu) = \frac{1}{eT\Omega} \int \sigma_{\alpha\beta}(\epsilon) (\epsilon - \mu) \left[ -\frac{\partial f_{\mu}(T, \epsilon)}{\partial \epsilon} \right] d\epsilon$ .

We first study the evolution of the electronic structure of the nanocomposites with increasing doping up to 32 pairs of dopant atoms in the 1000-atom supercell (6.4%), which is close to the optimal experimental doping of 5% - 6% [7]. We have run calculations for a 64-atom  $\text{PbTe}$  supercell containing one pair of doping atoms [(Ag,Sb), etc.] and obtained reduced band gaps (see Table I) compared to pure  $\text{PbTe}$ , which is consistent with previous calculations [14]. However, it is an artifact of using the small 64-atom supercell that incorrectly constrains the dopant-atom pairs into a chain model. Re-

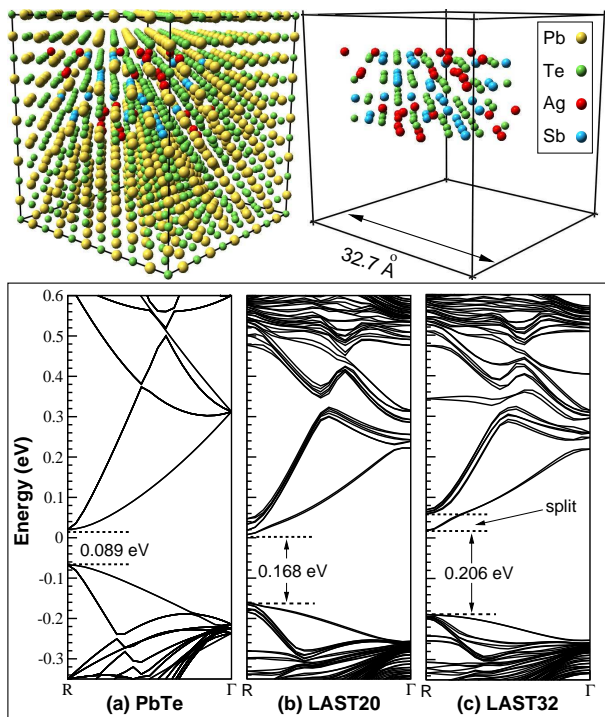


FIG. 1: (Color online) *Upper panel:* (Left) The cubic supercell (1000 atoms; side length 32.7 Å) of LAST holding a precipitate of size ( $\sim 2.5$  nm) comparable to those found in experiment. (Right) The  $\text{AgSbTe}_2$  nanoprecipitate containing 32 pairs of (Ag, Sb) dopant atoms. *Lower panel:* Calculated (with SOI) band structures for (a) PbTe, LAST with (b) 20 pairs, and (c) 32 pairs of Ag-Sb in the 1000-atom supercell.

moving such constraints by using the larger supercell, we find that the dopant atoms tend to form nanoclusters as observed in experiment [17]. Rising doping level drives a systematic trend of band-gap widening, which is directly correlated with the nanodopant-induced strain (up to 2%) that exists in a large volume (several times that of the nanodopant) and is highly inhomogeneous, which is consistent with experiment [24]. We have examined the effects of uniform lattice expansion and compression, several non-uniform lattice distortion modes, and compared results with or without lattice relaxation. The results indicate that the non-uniform lattice distortion is the driving force for the band-gap increase. The calculated band gap for LAST rises monotonically with doping from 0.089 eV for PbTe to 0.103, 0.168 and 0.206 eV for 4, 20, and 32 Ag-Sb pairs in the 1000-atom supercell, respectively. The same trend also holds for LBST, LANT, and LBNT. This represents a new mechanism of band-gap modulation in PbTe-based nanocomposites, which is different from those by uniform compression or temperature-driven lattice expansion and Debye-Waller effect [25]. In this work we focus on this new phenomenon and its effect on TE properties without explicit consideration of the temperature-driven effects. Our calculations

TABLE I: Calculated band gaps (in eV) for the nanodopant and single-pair model with 32 pairs and one pair of doping atoms in the 1000-atom and 64-atom supercell, respectively. The calculated band gap for undoped PbTe is 0.089 eV.

System	Nanodopant Model	Single-Pair Model
LAST	0.206	0.042
LBST	0.156	0.011
LANT	0.189	0.086
LBNT	0.124	0.073

underestimate the band gap of PbTe by about 50% compared to the experimental value of 0.19 eV [26], which is typical for density functional calculations [27]. Applying the same ratio to the nanocomposites, we estimate the band gaps for LAST, LBST, LANT and LBNT to be 0.41, 0.31, 0.38 and 0.25 eV, respectively. These results are in good agreement with recent experimental data on the values and trends of the band gap [28].

The band-edge states play a dominant role in determining electrical transport properties. Here we focus on LAST for a detailed analysis. Our calculations show (Fig. 1) that the dispersion of the LAST band-edge states undergoes relatively small changes despite the large band-gap widening. However, a doubly degenerate band splits off the original highly degenerate PbTe CBM band manifold. A close analysis of our calculated data shows that while strain-induced symmetry reduction generally leads to band splitting, its effect in nanocomposites is complicated by the inhomogeneous strain distribution. Consequently, we find that SOI in the nanodopant plays a dominant role in producing the larger splitting in LAST-type nanocomposites. This split-off reduces the density of states at the CBM. A band-composition analysis reveals that the split-off band contains a high (>30%) component of Sb  $p$ -states, which is similar to the case of atomic doping studied previously [13]. Meanwhile, the band-edge states near the valence band maximum (VBM), comprising predominantly Te  $p$ -states, largely maintain their dispersion behavior compared to PbTe.

The Ag atoms in LAST (and LBST) deviate significantly from the ideal lattice positions [Fig. 2(a)]. Meanwhile, Na atoms in LANT (and LBNT) bind strongly with the neighboring Te atoms and, consequently, are only slightly displaced [Fig. 2(b)]. Therefore, the Ag bonding states are expected to be shallower and closer to the VBM, similar to atomic doping case [13] while those of Na deeper in the valence band. This is verified by our calculations. Fig.2(c) and (d) show the calculated partial charge density of LAST and LANT within a 0.2-eV window below the VBM; one can see in the nanodopant region a strong presence of the Ag charge but an absence of the Na charge. These Ag-doping-induced states will enhance the density of states near the VBM of p-type

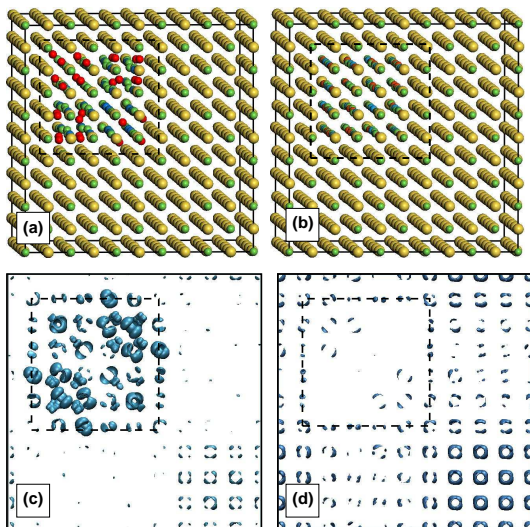


FIG. 2: (Color online) Crystal structure (supercell) of (a) LAST and (b) LANT and (c, d) their respective partial charge density (at isosurface of  $0.012 e/\text{\AA}^3$ ) within  $0.2 eV$  below the VBM. The dashed-line boxes outline the nanodopants.

LAST/LBST, making them good candidates for high-performance TE materials since p-type PbTe is already predicted to have high thermopower [29].

For narrow-gap semiconductors like PbTe, a sizable band-gap widening has significant influence on electrical transport properties. It is instructive to examine the temperature dependence of the integrand factors  $df/d\epsilon$  and  $(\epsilon - \mu)df/d\epsilon$ , which peak at or near the band edge (CBM for n-type and VBM for p-type materials). At high temperatures, the peak widths become larger than the narrow band gap and, consequently, an increase in band gap leads to a significant loss of contribution from the minority-carrier band, resulting in a decrease of  $\sigma$ . Meanwhile, since  $(\epsilon - \mu)df/d\epsilon$  is an odd function of  $\epsilon - \mu$ ,  $S$  receives positive and negative contribution from the carriers with energies above and below the chemical potential, which lies in the band gap in the present cases. A band-gap increase thus reduces the detrimental term from the minority-carrier band, thus yielding an enhancement of  $S$ . This analysis indicates that these band-gap effects on electrical transport properties will be more pronounced at higher temperatures with increasing band gaps, which is consistent with our calculations below.

A full electrical transport calculation for a large system like LAST is computationally unfeasible. We use PbTe as a surrogate and modify the host band structure to mimic the key features of the band modulations, namely the band-gap widening and band split-off at the CBM. This approach works here since the nanocomposite bands near the band edges, which are most responsible for the transport properties, undergo relatively small changes compared to those of PbTe. The band changes away from the band edges have little influence since the

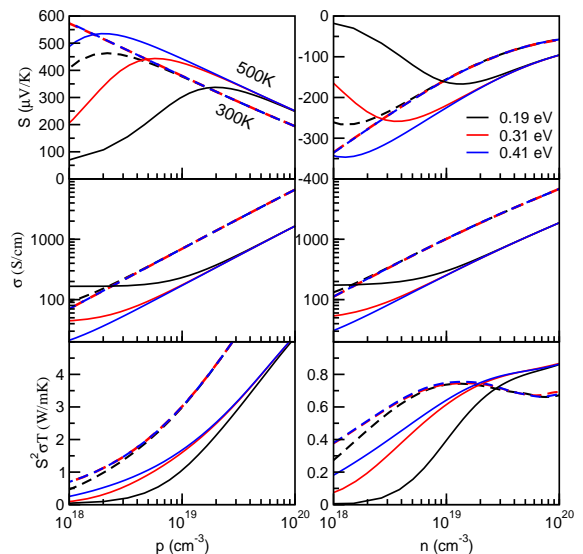


FIG. 3: (Color online) Calculated thermopower  $S$ , electrical conductivity  $\sigma$ , and  $S^2\sigma T$  as a function of carrier (p or n) concentration at the band gap of  $0.19, 0.31$  and  $0.41 eV$  for pure PbTe, LBST and LAST, respectively. The solid and dashed lines are for data at  $500 K$  and  $300 K$ , respectively.

integrand functions in the transport equations peak near the band edges and decrease rapidly. Despite expected quantitative deviations by factors not considered here (e.g., band-dispersion variations), this approach captures the main new physics and allows an assessment of the trends and mechanisms for electrical transport behavior. We calculate  $S$ ,  $\sigma$ , and the power factor  $S^2\sigma$  times  $T$  (PFT) using the Boltzmann transport theory. The WIEN2K is used for eigenvalue calculations on denser  $k$ -grids up to  $48 \times 48 \times 48$ . We calculate  $\sigma/\tau$ , where  $\tau$  is the relaxation time, which is obtained by fitting the experimental conductivity data of LAST [3]. The obtained energy independent values are  $3.304 \times 10^{-14} s$  at  $300 K$  and  $0.936 \times 10^{-14} s$  at  $500 K$ . It should be noted that these data reflect the effect of nanodopant-induced strain, which tends to reduce the relaxation time.

Our results (Fig. 3) show that at  $300 K$  the energy gap variation has little effect on  $S$ ,  $\sigma$ , and PFT except for an enhancement of  $S$  at low carrier concentrations around  $1 \times 10^{18} cm^{-3}$ . At  $500 K$ , the band gap effect becomes important at higher concentrations ( $\sim 10^{19} cm^{-3}$ ). The increased band gap leads to significantly enhanced  $S$  but reduced  $\sigma$ , which is expected from the temperature dependence of the integrand factors discussed above. They combine to produce a considerable (up to 70%) enhancement of the PFT. It is noted that the calculated PFTs are much larger for the p-type materials than those for the n-type. This is because the relaxation time  $\tau$  is obtained from fitting the experimental data for n-type LAST and the same  $\tau$  is used for both carriers. Modifications for p-type materials are expected when experimental data

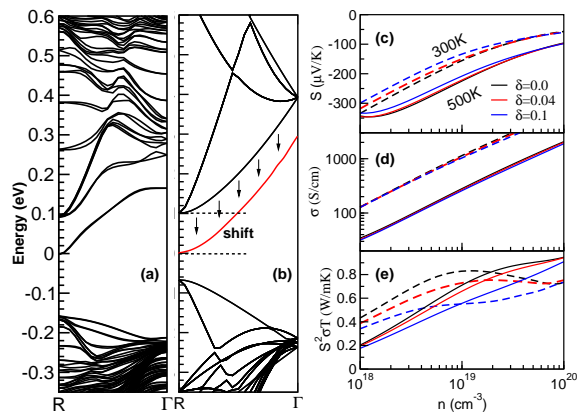


FIG. 4: (Color online) (a) Calculated (with SOI) band structure of LBST with 32 pairs of Ag-Bi in the 1000-atom supercell; (b) Illustration of the band shift  $\delta$  near the CBM of PbTe; (c-e)  $S$ ,  $\sigma$ ,  $S^2\sigma T$  versus  $n$  at  $\delta=0.0$ , 0.04, and 0.1 eV.

becomes available. Nevertheless, comparisons within the same carrier type are still meaningful.

The split-off of the doubly-degenerate state at the CBM reduces the density of states near the Fermi level, which would reduce  $S$  [30]. At 32 pairs of dopants, this band splitting is 0.04 eV for LAST [Fig. 1(c)] and 0.10 eV for LBST [Fig. 4(a)]. To evaluate its effect, we have carried out a series of calculations by shifting the lowest doubly-degenerate band of PbTe [as shown in Fig. 4(b)] by  $\delta = 0$  eV (PbTe), 0.04 eV (LAST), and 0.10 eV (LBST) while keeping the band gap constant (results in Fig. 4 (c-e) are for  $E_g = 0.41$  eV; other values of  $E_g$  produce the same trend). Increasing  $\delta$  leads to a decrease of both  $S$  and  $\sigma$ , which combine to produce a considerable reduction in PFT. It is noted that, unlike the band-gap effect discussed above, the effect of the band shift is pronounced at both 300 K and 500 K. This is because the reduction of density of states near the CBM has similar effects at different temperatures. Compared to LAST, the larger Bi-SOI-induced splitting in LBST yields lower density of states near the CBM and a smaller band gap, thus producing lower PFT, which is consistent with experimental observations [7].

The competing nature of the effects by nanodopant-induced band modulations constrains TE properties of LAST-type materials; however, optimizing PFT within such constraints is crucial to achieving high  $ZT$  in this class of thermoelectrics. Our results suggest two principles for PFT optimization: (1) the nanodopants should introduce large strain fields in the host lattice to increase the band gap and (2) dopant atoms should have weak SOI to minimize the band splitting at the CBM. These insights may also be useful for other narrow-gap semiconductor-based thermoelectrics. Several factors omitted in this work, such as the accurate value and temperature dependence of the energy gap and the band-edge-state dispersion variations, will affect some quanti-

tative aspects of our discussion but are not expected to change any conclusions on trends and mechanisms.

In summary, we show by first-principles calculations that nanodopants in  $\text{XPb}_m\text{YTe}_{2+m}$  ( $X=\text{Ag,Na}$ ;  $Y=\text{Sb,Bi}$ ) nanocomposites induce a large band-gap widening and a band splitting at the CBM. These band modulations have strong but competing influences on electron transport and TE properties. This new paradigm for nanodopant-induced band modulation in narrow-gap semiconductors has significant implications for research in this emerging field.

This work was supported by DOE Cooperative Agreements DE-FC52-06NA26274, DE-FC26-04NT42278 and by GM, and used resources of NCCS and CNMS at ORNL, sponsored by DOE Offices of Advanced Scientific Computing Research and Basic Energy Sciences.

- 
- [1] P. Y. Yu and M. Cardona, *Fundamentals of Semiconductors Physics and Material Properties*, (Springer-Verlag Berlin, Heidelberg, 2010)
  - [2] J. P. Heremans, C. M. Thrush, and D. T. Morelli, *Phys. Rev. B* **70**, 115334 (2004).
  - [3] K. F. Hsu, *et al.*, *Science* **303**, 818 (2004).
  - [4] E. Quarez, *et al.*, *J. Am. Chem. Soc.* **127**, 9177 (2005).
  - [5] P. F. P. Poudeu, *et al.*, *J. Am. Chem. Soc.* **128**, 14347 (2006).
  - [6] J. Androulakis, *et al.*, *Adv. Mater.* **18**, 4719 (2006).
  - [7] M. -K. Han, *et al.*, *Chem. Mater.* **20**, 3512 (2008).
  - [8] J. Q. He, *et al.*, *J. Am. Chem. Soc.* **131**, 17828 (2009).
  - [9] P. F. P. Poudeu, *et al.*, *Chem. Mater.* **22**, 1046 (2010).
  - [10] M. G. Kanatzidis, *Chem. Mater.* **22**, 648 (2010).
  - [11] W. Kim, *et al.*, *Phys. Rev. Lett.* **96**, 045901 (2006).
  - [12] S. V. Faleev and F. Léonard, *Phys. Rev. B* **77**, 214304 (2008).
  - [13] D. Bilc, *et al.*, *Phys. Rev. Lett.* **93**, 146403 (2004).
  - [14] K. Hoang, S. D. Mahanti, and M. G. Kanatzidis, *Phys. Rev. B* **81**, 115106 (2010).
  - [15] D. Bilc, S. D. Mahanti, and M. G. Kanatzidis, *Phys. Rev. B* **74**, 125202 (2006).
  - [16] H. Hazama, U. Mizutani, and R. Asahi, *Phys. Rev. B* **73**, 115108 (2006).
  - [17] X. Ke, *et al.*, *Phys. Rev. Lett.* **103**, 145502 (2009).
  - [18] S. V. Barabash, V. Ozolins, and C. Wolverton, *Phys. Rev. Lett.* **101**, 155704 (2008).
  - [19] J.P. Perdew, *et al.*, *Phys. Rev. B* **46**, 6671(1992).
  - [20] G. Kresse and J. Furthmüller, *Phys. Rev. B* **54**, 11169 (1996).
  - [21] G. Kresse and D. Joubert, *Phys. Rev. B* **59**, 1758 (1999).
  - [22] See details about Wien2K at [www.wien2k.at](http://www.wien2k.at)
  - [23] G. K. H. Madsen and D. J. Singh, *Comput. Phys. Commun.* **175**, 67 (2006).
  - [24] L. Wu, *et al.*, *J. Appl. Phys.* **105**, 094317 (2009).
  - [25] Y. W. Tsang and M. L. Cohen, *Phys. Rev.* **3**, 1254 (1971).
  - [26] C. R. Hewes, *et al.*, *Phys. Rev. B* **7**, 5195 (1973).
  - [27] M. S. Hybertsen and S. G. Louie *Phys. Rev. B* **34**, 5390 (1986).
  - [28] A. Gueguen, *et al.*, *Chem. Mater.* **21**, 1683 (2009); K. Ahn, *et al.*, *Chem. Mater.* **22**, 876 (2010).

- [29] D. J. Singh, Phys. Rev. B **81**, 195217 (2010).
- [30] M. Cutler and N. F. Mott, Phys. Rev. **181**, 1336 (1969).